# Journal of Materials Chemistry C

Accepted Manuscript


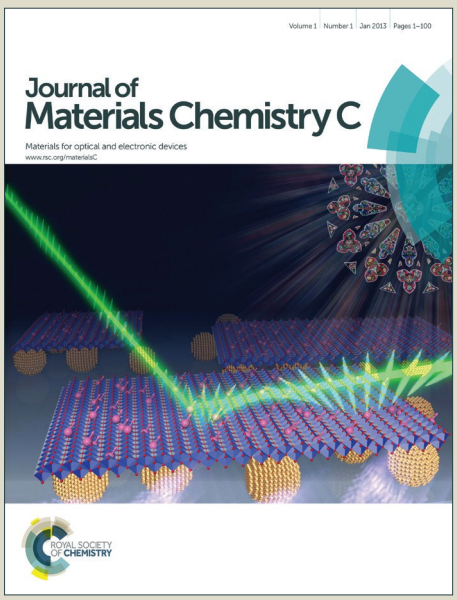



This is an *Accepted Manuscript*, which has been through the Royal Society of Chemistry peer review process and has been accepted for publication.

*Accepted Manuscripts* are published online shortly after acceptance, before technical editing, formatting and proof reading. Using this free service, authors can make their results available to the community, in citable form, before we publish the edited article. We will replace this *Accepted Manuscript* with the edited and formatted *Advance Article* as soon as it is available.

You can find more information about *Accepted Manuscripts* in the Information for Authors.

Please note that technical editing may introduce minor changes to the text and/or graphics, which may alter content. The journal's standard Terms & Conditions and the Ethical guidelines still apply. In no event shall the Royal Society of Chemistry be held responsible for any errors or omissions in this *Accepted Manuscript* or any consequences arising from the use of any information it contains.



ROYAL SOCIETY OF CHEMISTRY

www.rsc.org/materialsC

Journal Name

ARTICLE

# Color-Tunable and Single-Band Red Upconversion Luminescence form Rare-Earth Doped Vernier Phase Ytterbium Oxyfluoride Nanoparticles

Received 00th January 20xx,
Accepted 00th January 20xx

DOI: 10.1039/x0xx00000x

www.rsc.org/

Ting Wen, Yannan Zhou, Yanzhen Guo, Chunmei Zhao, Baocheng Yang and Yonggang Wang*

Rare-earth upconversion (UC) nanophosphors that can convert near-infrared excitations into visible light region are desirable for various applications such as photonics, photovoltaics and biological imaging. The choice of host lattices and the doping concentration of rare-earth ions are crucial for intense UC outputs and selective emission profiles. Here, we report the facile fabrication and UC performance of Vernier phase ytterbium oxyfluorides (*V*-YbOF) as a promising host lattice for the first time. The multiple doping sites with low symmetries ($C_1$ and $C_s$) in the *V*-YbOF structure and the layered Yb sublattice allowing high concentration of the sensitizer $Yb^{3+}$ are expected to give novel and preferable UC perforrmance. Experimentally, pure and rare-earth ($Ho^{3+}$, $Er^{3+}$, $Tm^{3+}$) doped *V*-YbOF nanoparticles were synthesized via a sol-gel process followed by subsequent fluorination treatment using polytetrafluoroethylene as the fluridizer. Tunable UC emissions with various red/green ratios were achieved in $Ho^{3+}$ doped *V*-YbOF nanoparticles under 980 nm excitation. Single-band red (~660 nm) UC luminescence and strong near-infrared emissions (centred at 700 and 805 nm) were observed in $Er^{3+}$ and $Tm^{3+}$ incorporated samples, respectively. The energy transfer mechanism was investigated by combined *P-I* measurements, lifetime evaluation and associated with the crystal structure feature. This work illustrates that, Yb-rich compounds with low-dimensional structure features are also promising candidates as UC host lattices for variety of applications.

## Introduction

Trivalent rare-earth ions ($RE^{3+}$) doped upconversion (UC) materials converting near-infrared (NIR) photons into visible emissions via the multi-photon process provide an attractive technique for various applications in solar cell, bio-sensing and bio-imaging.[1-6] Their intrinsic advantages, such as low bio-toxicity, narrow emission bandwidths, weak background autofluorescence and high penetration depth, make them superior to the conventional used organic fluorophores and quantum dots.[7-11] The most frequently studied UC materials are generally composed of *RE* ions and a host matrix for their spatially distribution, which makes the host materials essential for UC transitions and thus responsible for rational control over the emission profile and high emission efficiency.[12-16] Among the well-developed host materials, binary or ternary oxides and fluorides are testified to be effective for the UC generation of *RE* ions owing to their low phonon energies that can reduce the energy consumption in the energy transfer process.[4,5,12,17-21] *RE* oxyfluorides are also one of the most frequently adopted host materials for *RE* doping, which can often give intense and multifarious UC photoluminescence (PL) properties. The excellent UC performance benefits from their abundant structure types (*i.e.*: rhombohedral SmSI-type *R*-3*m*, tetragonal PbFCl-type *P*4/*nmm* and cubic fluorite-like *Fm*-3*m*) and ever-present low symmetry of $RE^{3+}$ due to the distortion in their crystal lattices.[22-33] For instance, a series of monodisperse *RE*OF (*RE* = La-Lu, Y) nanocrystals with diverse shapes were fabricated by Yan's group, and the cubic GdOF:Yb,Er nanocrystals showed intense UC green light under 980 nm excitation.[24,34] Comparatively, tetragonal $Gd_4O_3F_6$ and trigonal GdOF with Er/Tm/Yb codoping generated bright white light constituted with green, red and NIR UC emission.[30-32] Recently, intense ultraviolet/blue UC emissions were obtained in orthorhombic $Y_7O_6F_9$:Yb,Tm powders and strong NIR-to-visible UC fluorescence has been observed in cubic YOF:Yb, Er/YOF core-shell nanocrystalline structures.[35]

In our previous work, we reported $RE^{3+}$ doped Vernier phase $Y_6O_5F_8$ and $Lu_5O_4F_7$ (denoted as *V*-YOF and *V*-LuOF) nanocrystals showing intense and multicolor NIR to visible UC PL.[15,16] The orthorhombic crystal structure (*Pcmb*, *Abm*2) originates from the fluorite-type structure, which is proved to be the best host lattice currently (such as $CaF_2$ and

*Institute of Nanostructured Functional Materials, Huanghe Science and Technology College, Zhengzhou, Henan, 450006, China. *E-mail: yyggwang@gmail.com*

Electronic Supplementary Information (ESI) available: Refined structure details; schematic representation of Yb sublattice; CIE chromaticity diagram of $Ho^{3+}$ doped *V*-YbOF. See DOI: 10.1039/x0xx00000x

This journal is © The Royal Society of Chemistry 2015



Please do not adjust margins

Journal of Materials Chemistry C Accepted Manuscript

Na*RE*$F_4$),[12,14] but differs significantly from any other familiar structure types of *RE* oxyfluorides mentioned above. The assorted array of $O^{2-}$ and $F^-$ ions in the $a \times nb \times c$ unit cell offers highly disordered host lattice, which provides several multiple low symmetry crystallographic sites ($C_1$, $C_2$ and $C_s$) suitable for *f-f* transitions of the $RE^{3+}$ dopants and thus gives rise to intense UC luminescence.[47] Multicolor outputs (purple, green, red and yellow) with strong intensities were observed in the $Yb^{3+}/RE^{3+}$ (*RE* = Ho/Er/Tm) codoped *V*-YOF and *V*-LuOF phosphors, respectively. Notably, the $Yb^{3+}/Er^{3+}$ codoped *V*-LuOF yields a nearly single-band red emission at about 660 nm. These results illustrate that the Vernier phase *RE* oxyfluorides are promising as host materials for the generation of UC PL.

Owing to the sufficient absorption cross-section in the NIR spectral region (~980 nm), $Yb^{3+}$ ions are frequently adopted as sensitizers for $Ho^{3+}/Er^{3+}/Tm^{3+}$ activators to achieve high-efficiency UC emission. Whereas, the $Yb^{3+}$ doping concentration is highly restricted in most common host materials (< 20 mol%), for that high doping level of $Yb^{3+}$ is likely to arouse appreciable quenching of UC PL owing to the increased probability of random energy migration to lattice or surface defects.[11,36,37] Due to this reason, Yb based compounds are always ruled out from candidates as host materials for UC generation. However, the use of low-dimensional host materials rather than those with high symmetry (*e.g.* cubic $NaYF_4$) to disfavor the random energy migration may be feasible to minimize the concentration quenching problem. In a recent example, Liu's group proposed orthorhombic $KYb_2F_7$ as a unique host material with clustered Yb sublattice to realize high sensitizer concentration.[38] In the crystal structure of $KYb_2F_7$, the average distance between the tetrahedral $Yb^{3+}$ clusters is larger than that within the clusters, and thus no concentration quenching was observed in the $Yb^{3+}$ concentration range from 18% to 98%. While in other investigations, it's found that the increase of $Yb^{3+}$ concentration can shorten the energy transfer operating distance and thus vary the radioactive transitions from high-lying excited states.[39] As a result, UC emissions with diverse colors and different intensities have been observed.[40-43] For example, an enhanced red emission in α-$NaYF_4$:Yb,Er nanocrystals was observed when the $Yb^{3+}$ doping ratio was increased from 25% to 60%, which could be attributed to the energy back transfer process (EBT) from $Er^{3+}$ to $Yb^{3+}$ with the decreased inter atomic distance between $Yb^{3+}$ and $Er^{3+}$.[6] Continuous color-tunable UC PL was achieved by increasing $Yb^{3+}$ concentrations in monoclinic $Gd_2O_3$:$Yb^{3+}/Er^{3+}$ according to the phonon-assisted EBT process.[44] A significantly enhanced NIR-to-NIR UC PL was observed in $NaYF_4$:$Yb^{3+}/Tm^{3+}$ nanocrystals by increasing $Yb^{3+}$ concentration from 20% to 98%.[45] And the enhancement was attributed to the increased excitation absorption and energy transfer efficiency between $Yb^{3+}$ and $Tm^{3+}$ ions. Therefore, it is possible to realize tunable multi-color UC outputs in Yb-based low-dimensional host lattices only if the concentration quenching effect is minimized to a low level.

In this article, we demonstrate that Vernier phase ytterbium oxyfluoride (*V*-YbOF) with a two-dimensional (2D) Yb sublattice can be used as a novel host material for UC PL generation of *RE* ions. Through a sol-gel process followed by subsequent low-temperature fluorination, pure and $RE^{3+}$ (*RE* = Ho/Er/Tm) doped orthorhombic *V*-YbOF samples were fabricated. The products are characterized by means of PXRD, TEM, SAED and PL spectroscopy, respectively. Tunable, single-band red and intense NIR UC emissions have been achieved in the as-obtained materials and the novel optical properties are associated with the 2D and disordered crystal structure features. This result indicates that these Vernier phase *RE* oxyfluorides are promising host materials for the generation of UC luminescence for modern bio-imaging and bio-sensing applications.

## Experimental

**Material syntheses.** Undoped *V*-YbOF powders were synthesized via a low-temperature fluorination route by adopting $Yb_2O_3$ as the raw materials and polytetrafluoroethylene (PTEF) as fluridizer.[46,47] In a typical synthesis procedure of *V*-YbOF, 0.394 g $Yb_2O_3$ (0.001 mol; >99.5% purity) and 0.11 g PTEF powder (0.0022 mol $CF_2$; >99% purity) were weighted and grounded together with ethanol for several minutes. The resulting fine powder was placed in an alumina crucible and then sealed partially by an alumina cover. The sample was slowly heated to 550 °C at a heating rate of 5 °C/min. After holding at the highest reacting temperature for 4 hours, the furnace was allowed to cool down to room temperature naturally. Experimental attempts with different $Yb_2O_3/CF_2$ ratios or at various heating processes were conducted following similar procedure.

$RE^{3+}$-doped *V*-YbOF powders were fabricated by a sol-gel method followed with the fluorination process. Firstly, proportional $RE_2O_3$ (*RE* = Ho, Er, Tm) were mixed with $Yb_2O_3$, and dissolved in hot nitric acid to form a clear solution. Then excessive citric acid was added under stirring. After that, the solution was heated at 80, 120, 160, 200, 240, 280, 320 °C for 2 hours at each step and finally heated at 800 °C for 5 hours. The resulting powders were mixed with PTEF and followed the similar procedure as undoped *V*-YbOF to generate $RE^{3+}$-doped *V*-YbOF samples. $RE^{3+}$ doped *V*-YOF and hexagonal $NaYF_4$ for comparison purpose were synthesized following some previous works.[15,47]

**Characterization.** Powder X-ray diffraction (PXRD) data of all the samples were collected at room temperature (25 °C) on a Bruker D8 Advance diffractometer using a germanium monochromatic (Cu K$\alpha$). The data in the 2$\vartheta$ range of 5-130° were collected in a step of 0.02° with the remaining time 1 s per step under the tube conditions 40 kV and 40 mV. The least-squares refinements of the cell dimensions and atomic positions of all of the samples were performed adopting the previously reported structural parameters of $Y_6O_5F_8$ as the initial model.[48]

Transmission electron microscopy (TEM) and selected-area electron diffraction (SAED) images were performed on a transmission electron microscope (Tecnai G2 20, S-TWIN) with an accelerating voltage of 200 kV. Elemental analysis was also performed by energy dispersive X-ray spectroscopy (EDX) on the same instrument. The UC PL spectra were recorded at room temperature on a modified Hitachi F-4500 spectrophotometer with a tunable 10 W 980 nm laser diode (Lasever Inc.) as the excitation source. The UC PL decay curves were measured by using a FLS980 spectrophotometer equipped with a 150 W Xe lamp as the

Journal of Materials Chemistry C Accepted Manuscript


This journal is © The Royal Society of Chemistry 2015

excitation source. All of the measurements were performed at room temperature.

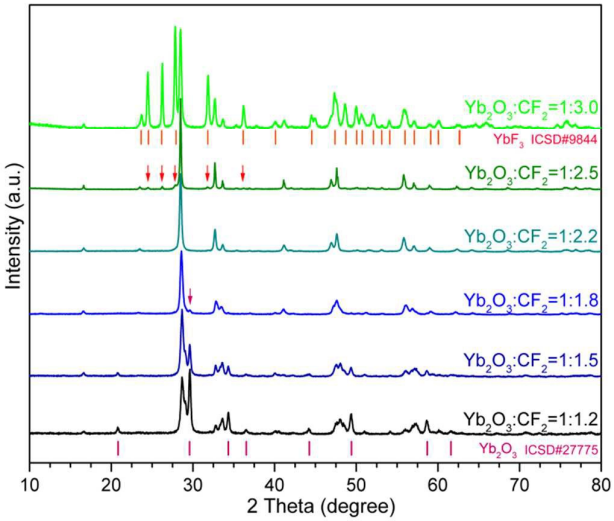


**Fig. 1** Powder X-ray diffraction patterns of as-synthesized *V*-YbOF with various $Yb_2O_3$/PTEF ratios. The short vertical bars represent the main theoretical Bragg reflection positions of cubic $Yb_2O_3$ (ICSD#27775) and $YbF_3$ (ICSD#9844).

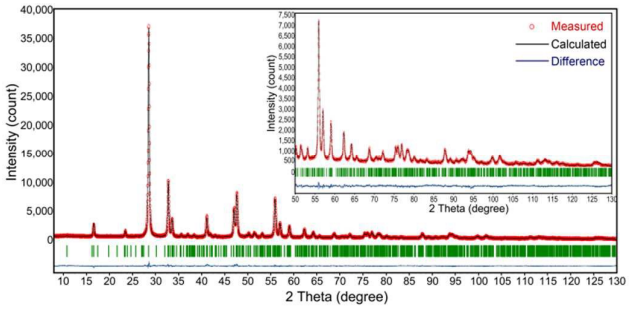


**Fig. 2** Rietveld refinement based on the powder X-ray diffraction data of the undoped $Yb_6O_5F_8$ with the $Yb_2O_3$/PTEF ratio of 1:2.2 (mol/mol). The inset shows the details of powder X-ray diffraction data and rietveld refinement results in the range of 50-130°.

## Results and discussion

**Synthesis, crystal structure and morphology.** Phase-pure *V*-YbOF powders were obtained by adopting $Yb_2O_3$ as the raw materials and polytetrafluoroethylene (PTEF) as fluridizer. It's found that, the formation of pure *V*-YbOF samples relies much on the heating procedure, the highest sintering temperature, the holding time and particularly the Yb/F ratios. **Fig. 1** shows the PXRD patterns of the products from proportional $Yb_2O_3$ and PTEF in partially sealed crucible at 550 °C for 4 hours. Unreacted $Yb_2O_3$ could be observed in the products until 80% excess PTEF was used (Yb/F = 1:1.8). While in the case with 150% excess PTEF, $Yb_2O_3$ was over fluoridated to $YbF_3$. A Yb/F ratio around 1:2.2 was found appropriate to produce phase-pure *V*-YbOF in this specific experimental conditions.

The Vernier phase lanthanides oxyfluorides ($RE_nO_{n-1}F_{n+2}$, where *n* is an integer) are known only for small $Y^{3+}$ and $Lu^{3+}$ and there is no report of Yb isologues up to now. For the as-obtained samples, the simple cubic or tetrahedral *RE*OF structure types can be ruled out firstly by XRD peaks indexing. Then the *n* = 6 Vernier phase with formula $Yb_6O_5F_8$ was roughly assigned to the samples, which was supported by the results of both elemental measurements (average Yb/O/F = 1.18/1/1.67 by EDX, **Table S1**) and the cell parameter refinements. In order to further investigate the structure and properties, Rietveld refinement was performed using $Y_6O_5F_8$ (ICSD #68950)[48] used as an initial structure model. Accordingly, the O/F distribution and disorder of the structure were also treated by simply following those of $Y_6O_5F_8$. The refinement plot and structure of Vernier phase $Yb_6O_5F_8$ are shown in **Fig. 2**. The host material crystallizes in the centrosymmetric orthorhombic space group *Pcmb* and has an elongated *a* × *nb* × *c* unit cell (*n* = 6) derived from a fluorite-type structure, where *a* = 5.3323(7) Å, *b* = 6 × 5.4581(5) Å, and *c* = 5.4676 (8) Å. There are four crystallographic positions offered by the assorted array of $O^{2-}$ and $F^-$ ions for the 8-fold coordinated $Yb_6O_5F_8$ ions in the lattice, and they are arranged alternately along the *b*-axis. The detailed atomic positions and other structural parameters of the *V*-YbOF are listed in **Table S2**. The static distribution of O3 and F1 in the 8*d* position is treated in the same way as those in the *V*- YOF structure, and the isotropic temperature factors are fixed for all the atoms.

The representative crystal structure of the *V*-YbOF is shown in **Fig. 3a**. This orthorhombic structure adopting the space group *Pcmb* possesses an elongated *a* × *nb* × *c* super cell along the *b*-axis, where the values of *a*, *b* and *c* are very close, corresponding to the parameters of the parent cubic fluorite structure. The assorted array of $O^{2-}$ and $F^-$ anions is rather complex on account of both their semi-commensurate periodicity relative to that of the cations and the statistical disordered distribution in the 8*e* sites. This gives rise to four different Yb positions coordinated by eight oxide and/or fluoride ions: Yb1 in $C_2$ symmetric sites, Yb2 and Yb3 in $C_1$ sites, and Yb4 in $C_s$ sites, and thus different coordination environments for possible $RE^{3+}$ cations substitution, as shown in **Fig. 3b**. In the orthorhombic *V*-YbOF, the Yb atoms also arrange in a two-dimensional (2D) layered manner as shown in **Fig. S1**, where the distance between two neighbouring $Yb^{3+}$ ions (3.51-3.63 Å) is much shorter than the interlayer distance (4.02-4.10 Å). According to the formula of energy transfer probability $P_{ET}$ between two adjacent $Yb^{3+}$ ions:

$$P_{ET} = C_{Yb\text{-}Yb} \exp(-2R/L)$$ [38]

Here, *R* is the distance between the donor-acceptor pair, $C_{Yb\text{-}Yb}$ is the Yb-Yb interaction constant, and *L* is the effective Bohr radius (estimated to be ~0.3 Å for Yb-Yb interaction). The probability of energy transfer within the layer is one order of magnitude higher than that of interlayer energy transfer, which may decrease the UC concentration quenching of their lanthanide doped phosphors. This makes low-dimensional Yb-based compounds possible to be adopted as UC host materials.

For $RE^{3+}$ (*RE* = Ho, Er, Tm) doped samples, lanthanides mixed $Yb_2O_3$ are prefabricated by a modified sol-gel method at 800 °C firstly, then follow the same fluorination process as mentioned above. Powder XRD patterns of $Er^{3+}$ (2-12 mol %) -doped *V*-YbOF samples (**Fig. 4a**) show peak positions and intensities

Journal of Materials Chemistry C Accepted Manuscript



Please do not adjust margins

that can be well coincide with *V*-YbOF. The variation of unit cell volume according to the Rietveld refinement results is shown in **Fig. 4b**. When $Yb^{3+}$ positions were occupied by more

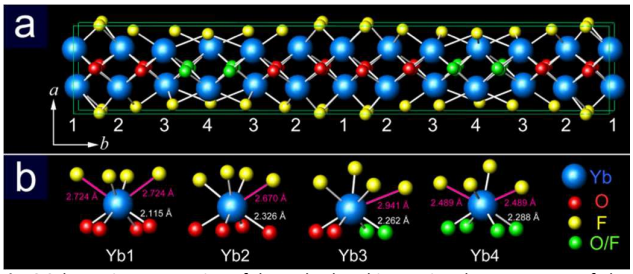


**Fig. 3** Schematic presentation of the orthorhombic Vernier phase structure of $Yb_6O_5F_8$ and the possible sites for $RE^{3+}$ doping. (a) The $a \times nb \times c$ unit cell with $n = 6$ along the *b*-axis, (b) the assorted array of $O^{2-}$ and $F^-$ ions offers four different types of $Yb^{3+}$ cation sites . Note that the $O^{2-}$ and $F^-$ anions located at 8*e* sites shown as green balls are of disordered distribution.

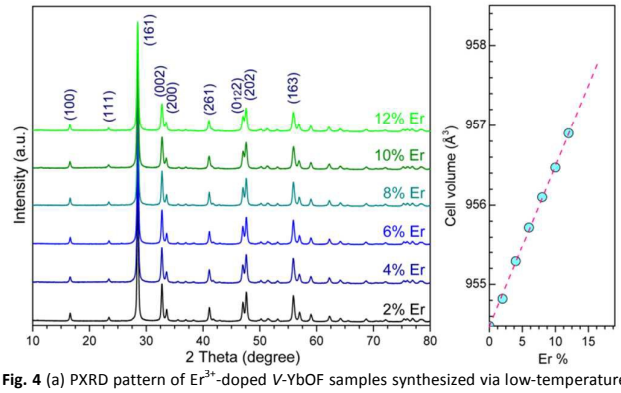


**Fig. 4** (a) PXRD pattern of $Er^{3+}$-doped *V*-YbOF samples synthesized via low-temperature fluoridation from the raw materials of oxides by using PTEF as fluridizer. (b) The variation of unit cell volume of $Er^{3+}$-doped *V*-YbOF with the increase of Er doping, according to the results of Rietveld refinement.

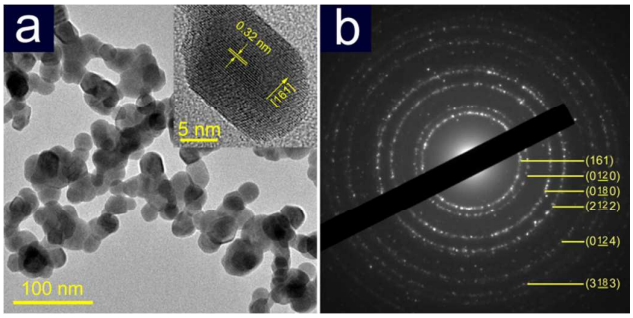


**Fig. 5** (a) TEM and (b) SAED images of $RE^{3+}$ doped *V*-YbOF nanoparticles.

and more $Er^{3+}$ ions, the cell volume of the solid solution increased gradually from 954.5 to 957.0 $Å^3$ due to the larger radius of $Er^{3+}$ ions (0.890 Å) compared with $Yb^{3+}$ ions (0.868 Å). And they show linear relationship following the Vegard's law for a solid solution. Thus, the low-temperature fluorination method provides us a facile route to achieve *V*-YbOF with high-purity and endows the feasibility of our evaluation upon $RE^{3+}$ doped *V*-YbOF serving as UC host materials.

**Fig. 5a** shows the typical transmission electron microscopy (TEM) image of the as-synthesized $RE^{3+}$-doped *V*-YbOF particles. They are well-proportioned nanoparticles with a mean size of approximate 40 nm in diameter, since the $RE^{3+}$ doped $Yb_2O_3$ precursors are prepared by adopting the sol-gel method. The high-resolution TEM images of individual $RE^{3+}$-doped *V*-YbOF nanocrystals reveal lattice fringes with a *d* spacing of 0.32 nm, which is well consistent with the distance of {161} facets of *V*-YbOF. Selected-area electron diffraction (SAED) patterns obtained from a large area of the particles confirms the monoclinic structure again and also phase-purity of the as-obtained bulk samples (**Fig. 5b**).

**UC PL of $RE^{3+}$-doped *V*-YbOF (*RE* = Ho, Er, Tm). Fig. 6a** displays the room-temperature UC emission spectrum of $Ho^{3+}$ doped *V*-YbOF samples under excitations of $\lambda_{ex}$ = 980 nm. The emission spectra were normalized to $Ho^{3+}$ emission at 540 nm for clarity and the relative UC PL intensities as a function of the $Ho^{3+}$ doping concentration were provided in Fig. S2. The two UC peaks at 540 and 670 nm can be assigned to $^5F_4$, $^5S_2 \rightarrow {}^5I_8$ and $^5F_5 \rightarrow {}^5I_8$ transitions of $Ho^{3+}$ ions respectively. It is significant that the intensity of the green band and red band can be tuned by simply varying the $Ho^{3+}$ doping concentration. As shown in **Fig. 6b**, along with the increase of $Ho^{3+}$ doping concentrations from 0.2 to 6 mol%, the green/red ratio of the UC intensities increased from 0.4 to about 6 and the output colour changed obviously from yellow to green accordingly. The dependence of the green-to-red intensity ratio on the concentration of $Ho^{3+}$ in the *V*-YbOF:Ho nanoparticles should be attributed to the different population states of $^5F_4/^5S_2$ and $^5F_5$ levels along with the change of average $Yb^{3+}$-$Ho^{3+}$ distance and the transition probability between them. The corresponding CIE chromaticity diagram of *V*-YbOF:Ho (0.2-6 mol%) nanoparticles was provided in **Fig. S3**.

**Fig. 7** displays the UC PL spectra of $Er^{3+}$ and $Tm^{3+}$ doped *V*-YbOF samples and their emission intensity as a function of $RE^{3+}$ doping concentration. For $Er^{3+}$ doped *V*-YbOF samples (2-12 mol %), single-band red emissions centered at 660 nm are observed, which can be ascribed to the typical $^4F_{9/2} \rightarrow {}^4I_{15/2}$ transitions of $Er^{3+}$ and the maximum UC output was achieved when the $Er^{3+}$ doping concentration is about 4 mol%. While in $Tm^{3+}$ doped *V*-YbOF samples, NIR emissions centered at 694 and 805 nm can be assigned to the $^3F_3 \rightarrow {}^3H_6$ and $^3H_4 \rightarrow {}^3H_6$ transitions of $Tm^{3+}$ ions, respectively. The maximum UC output at 805 nm is achieved when the doping concentration of $Tm^{3+}$ reaches 1 mol %.

Single-band red and NIR outputs are favored for their feasible utilities as optical imaging probes in bioapplications.[49] Such distinct outputs from the as-prepared $Er^{3+}$ and $Tm^{3+}$ doped *V*-YbOF phosphors could be primary attributed to the high density of $Yb^{3+}$ in the host lattice. Considering the high possibility of energy transfer between $Yb^{3+}$ and $RE^{3+}$ in such a $Yb^{3+}$-rich host lattice, the probability of EBT process from $RE^{3+}$ to the sensitizer $Yb^{3+}$ ions should be also highly enhanced.[6,39,44] **Fig. 8a** shows the details of the UC energy transfer mechanism of $RE^{3+}$ ($Ho^{3+}$, $Er^{3+}$, $Tm^{3+}$) doped *V*-YbOF samples. The EBT processes should have an exponential relationship with the number of involved photons, and will mainly affect the *f*-*f* transitions from higher energy level of the activators to the ground states. For instance, in the $Er^{3+}$ doped *V*-YbOF phosphors, the high concentration of $Yb^{3+}$ ions greatly facilitated

Journal of Materials Chemistry C Accepted Manuscript



This journal is © The Royal Society of Chemistry 2015

Please do not adjust margins

the EBT process and the photon excitation to higher $^2H_{9/2}$, $^2H_{11/2}$ and $^4S_{3/2}$ levels was suppressed, which results in the absence of blue ($^2H_{9/2}\rightarrow{}^4I_{15/2}$) and green ($^2H_{11/2}$,$^4S_{3/2}\rightarrow{}^4I_{15/2}$) emissions. While, in $Tm^{3+}$ doped samples, most of the excited phonons at $^1D_2$ and $^1G_4$

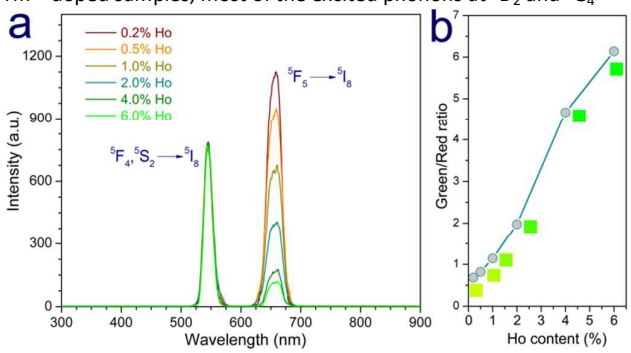


**Fig. 6** (a) UC emission spectra of *V*-YbOF:Ho (0.2-6 mol%) samples under 980 nm excitation (~ 3 W/cm$^2$). The emission spectra were normalized to $Ho^{3+}$ emission at 540 nm. (b) The variation of green/red ratio (according to the ratio of the intensity values at 540 nm to 670 nm) of the outputs from *V*-YbOF:Ho (0.2-6 mol%) nanoparticles.

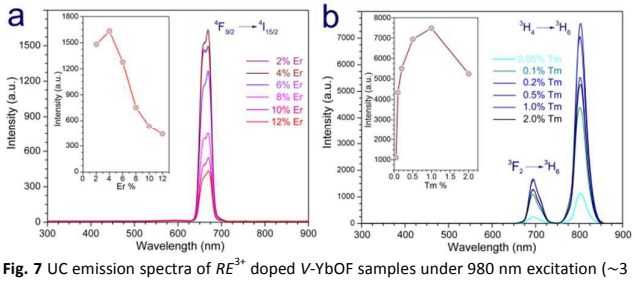


**Fig. 7** UC emission spectra of $RE^{3+}$ doped *V*-YbOF samples under 980 nm excitation (~3 W/cm$^2$) and the emission intensity variations of $RE^{3+}$ doped *V*-YbOF samples with the increase of $RE^{3+}$ doping concentration (the inserts): (a) *V*-YbOF:Er (2-12 mol %), (b) *V*-YbOF:Tm (0.05-2 mol %).

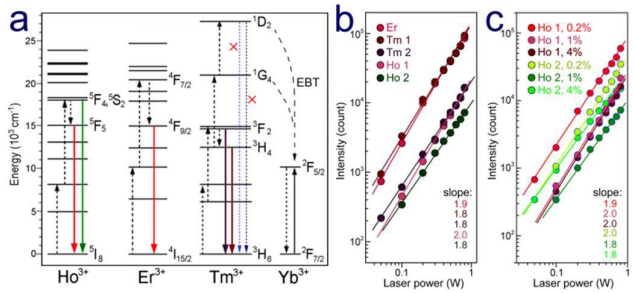


**Fig. 8** (a) Schematic energy level diagrams of the *f–f* transitions and EBT processes corresponding to the main UC bands. Log-log plots of the UC emission intensity *versus* the excitation power density under 980 nm excitation for: (b) 4%$Er^{3+}$, 1%$Tm^{3+}$, 1%$Ho^{3+}$ doped *V*-YbOF samples and (c) $Ho^{3+}$doped *V*-YbOF nanocrystals with different $Ho^{3+}$ doping concentrations. (Er: $^4F_{9/2}\rightarrow{}^4I_{15/2}$; Tm1: $^3H_4\rightarrow{}^3H_6$, Tm2: $^3F_3\rightarrow{}^3H_6$; Ho1: $^5F_5\rightarrow{}^5I_8$, Ho2: $^5F_4$, $^5S_2\rightarrow{}^5I_8$).

jump back to $Yb^{3+}$ and the three- or four-phonons involved $^1D_2\rightarrow{}^2F_{7/2}$ and $^1G_4\rightarrow{}^2F_{7/2}$ UC emissions are absent. In addition to the high concentration of $Yb^{3+}$ ions, the small radius of the $Yb^{3+}$ ion give rise to a short $Yb^{3+}$–$Yb^{3+}$ distance in the host lattice and thus leads to a short inter-atomic distances between $Yb^{3+}$ and $RE^{3+}$, which also facilitates EBT from $RE^{3+}$ to the sensitizer $Yb^{3+}$ and the formation of the single-band red and NIR emissions.[50]

In order to determine the energy transfer mechanism responsible for the UC processes, we investigated the pumping power dependence of the PL intensity (*P-I* curve). Fig. 8b shows the UC PL intensity versus the excitation power density on a double logarithmic scale for the emission bands ($Er^{3+}$: $^4F_{9/2}\rightarrow{}^4I_{15/2}$; $Tm^{3+}$: $^3H_4\rightarrow{}^3H_6$, $^3F_3\rightarrow{}^3H_6$; $Ho^{3+}$: $^5F_5\rightarrow{}^5I_8$, and $^5F_4$, $^5S_2\rightarrow{}^5I_8$) in the *V*-YbOF phosphors under excitation at 980 nm. The values measured for the

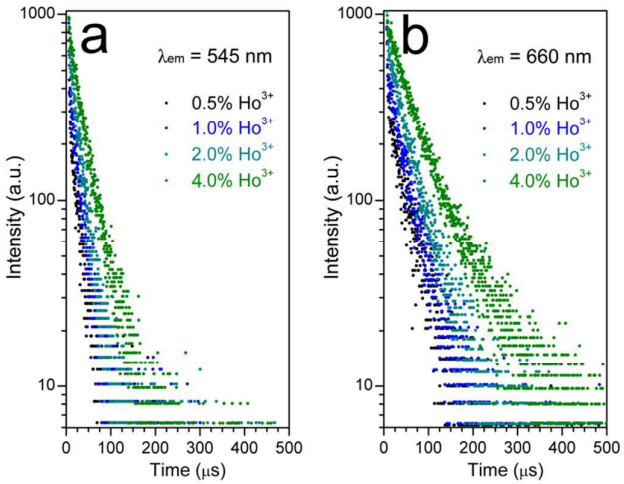


**Fig. 9** Decay curves for the UC luminescence of $Ho^{3+}$ doped *V*-YbOF samples with different $Ho^{3+}$ doping concentration: (a) Green emission at 545 nm ($^5F_4$, $^5S_2\rightarrow{}^5I_8$), (b) Red emission at 660 nm ($^5F_5\rightarrow{}^5I_8$).

slopes of the above emissions are 1.9 for $^4F_{9/2}\rightarrow{}^4I_{15/2}$ of $Er^{3+}$, 1.8 for $^3H_4\rightarrow{}^3H_6$, $^3F_3\rightarrow{}^3H_6$ of $Tm^{3+}$, 2.0 for $^5F_5\rightarrow{}^5I_8$ and 1.8 for $^5F_4$, $^5S_2\rightarrow{}^5I_8$ $Ho^{3+}$. It is known that the output UC emission intensity (*I*) is proportional to the pump power (*P*) via the following formula: $I\propto P^n$, where *n* is the number of pump photons required to populate the upper emitting level, which corresponds to the slope in the double-logarithmic coordinate. Accordingly, the observed slopes (*n* ~ 2) for the emission bands suggest that they all involve a two photon process. This simultaneously indicates the highly selective population of excited electrons on the $^4F_{9/2}$ energy level of $Er^{3+}$ and $^3H_4$, $^3F_3$ of $Tm^{3+}$ ions. Besides, we also measured the *P-I* curves of $Ho^{3+}$doped *V*-YbOF nanocrystals with various doping concentration of 0.1, 1 and 4 mol% to get further insight into the tunable green/red ratio of the UC emissions. The slopes all distribute around 2, indicating a two-photon absorption process in the UC generation. These results also support the above-proposed EBT process in $RE^{3+}$ doped *V*-YbOF phosphors and shed light on these Yb-rich oxyfluorides as novel host materials for desirable UC generation.

To further understand the dependence of R/G ratios on $Ho^{3+}$ doping concentrations associated with the energy transfer process, UC PL decay curves were measured on some $Ho^{3+}$-doped *V*-YbOF samples and the results are provided in **Fig. 9**. For the *x*%$Ho^{3+}$-doped *V*-YbOF (*x* = 0.5, 1.0, 2.0 and 4.0), near single exponential decay processes are observed. The lifetime values are calculated and shown in **Table S3**. It is evident that in a given sample with the same $Ho^{3+}$ content, the lifetime of $^5F_4$/$^5S_2$ (660 nm) are longer than that of $^5F_5$ (545 nm). The EBT-forbidden excited energy level $^5F_5$ exhibiting a longer lifetime indicates that the EBT process also possibly occurs in $Ho^{3+}$-doped V-YbOF. Along with the $Ho^{3+}$ contents increasing, the decay processes from both excited energy levels become slower, which can attribute to the enhanced possibility of the energy transfer between $Ho^{3+}$ and $Yb^{3+}$. All these evidences

Journal of Materials Chemistry C Accepted Manuscript



Please do not adjust margins

point to the EBT-assistant UC PL mechanism in $RE^{3+}$ doped V-YbOF nanoparticles.

Finally, the UC PL profiles of as-fabricated $RE^{3+}$ doped V-YbOF samples were compared with $RE^{3+}$ doped Vernier phase YOF and hexagonal $NaYF_4$. The former (20% Yb doped) is of similar crystal structure with *V*-YbOF but with slightly changed cell size and different Yb concentrations,[16] while the latter is the most efficient

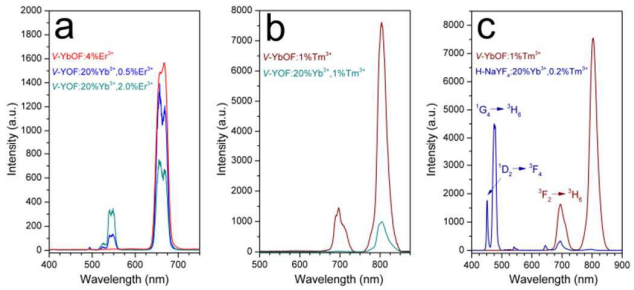


**Fig. 10** Comparison of the UC PL profiles between $RE^{3+}$-doped *V*-YbOF (*RE* = Er, Tm) and other host materials (*V*-YOF and hexagonal $NaYF_4$) under the same experimental conditions at room temperature.

UC host material currently. First of all, the 4%$Er^{3+}$-doped V-YbOF shows a purer single-band red and more intense UC emission than that of the 20%$Yb^{3+}$,*x*%$Er^{3+}$-doped V-YOF (*x* = 0.5, 2.0, **Fig. 10a**). Secondly, higher $Er^{3+}$ doping concentration is enabled due to the higher $Yb^{3+}$ contents in the lattice without obvious quenching of the UC emission. For the 1%$Tm^{3+}$-doped samples (**Fig. 10b**), *V*-YbOF shows more intense NIR UC emission around 800 nm than that of *V*-YOF and the emerging $^3F_2 \rightarrow {}^3H_6$ emission of $Tm^{3+}$ is caused by the increased population probability of the phonons on the $^3F_2$ level. In **Fig. 10c**, it can be seen that the 1%$Tm^{3+}$-doped *V*-YbOF presents distinct UC PL profile compared with that of 20%$Yb^{3+}$,0.2%$Tm^{3+}$-doped H-$NaYF_4$. The intense NIR output makes the material desirable for various bio-applications.

## Conclusions

In summary, we reported a low temperature fluorination route to fabricate Vernier phase ytterbium oxyfluoride as a novel UC host material. The $Ho^{3+}$ and $Er^{3+}$ doped phosphors present color-tunable (yellow to green) and single-band red emission, respectively. The $Tm^{3+}$ doped samples show intensive NIR-to-NIR UC PL around 800 nm. The assorted array of $O^{2-}$ and $F^-$ ions gives rise to the highly disordered host crystal structure and provides multiple low symmetry crystallographic sites suitable for $RE^{3+}$ doping. The layered arrangement of Yb sublattice may avoid the concentration quenching effect to a certain extent in these $RE^{3+}$ doped phosphors. Furthermore, the high concentration of $Yb^{3+}$ in the host lattice was considered as the primary factor for single-band and NIR emitting in accordance with EBT effect. The UC PL processes and the energy transfer mechanism were studied thoroughly by combined *P-I* and decay curve characterizations. We believe further research attentions on *V*-YbOF and other Yb-based host materials with low-dimensional structures will greatly boost the development of high-efficiency and single-band emitting UC phosphors in bioprobe and display applications.

## Acknowledgements

This work was supported by the National Natural Science Foundation of China (21301063, 51472102).

## Notes and references


1 J. C. G. Bünzli and C. Piguet, *Chem. Soc. Rev.*, 2005, **34**, 1048.
2 F. Wang and X. Liu, *Chem. Soc. Rev.*, 2009, **38**, 976.
3 M. Haase and H. Schäfer, *Angew. Chem. Int. Ed.*, 2011, **50**, 5808.
4 L. Wang, P. Li and Y. Li, *Adv. Mater.*, 2007, **19**, 3304.
5 C. Jiang, F. Wang, N. Wu and X. Liu, *Adv. Mater.*, 2008, **20**, 4826.
6 F. Wang and X. Liu, *J. Am. Chem. Soc.*, 2008, **130**, 5642.
7 S. V. Eliseeva and J. C. G. Bünzli, *Chem. Soc. Rev.*, 2010, **39**, 189.
8 Y. I. Park, J. H. Kim, K. T. Lee, K. S. Jeon, H. B. Na, J. H. Yu, H. M. Kim, N. Lee, S. H. Choi, S. I. Baik, H. Kim, S. P. Park, B. J. Park, Y. W. Kim, S. H. Lee, S. Y. Yoon, I. C. Song, W. K. Moon, Y. D. Suh and T. Hyeon, *Adv. Mater.*, 2009, **21**, 4467.
9 D. K. Chatterjee, M. K. Gnanasammandhan and Y. Zhang, *Small*, 2010, **6**, 2781.
10 L. Wang and Y. Li, *Chem. Commun.*, 2006, 2557.
11 Z. Gu, L. Yan, G. Tian, S. Li, Z. Chai and Y. Zhao, *Adv. Mater.*, 2013, **25**, 3758.
12 G. Wang, Q. Peng and Y. Li, *J. Am. Chem. Soc.*, 2009, **131**, 14200.
13 G. Wang, Q. Peng and Y. Li, *Chem. Commun.*, 2006, **46**, 7528.
14 F. Wang, Y. Han, C. S. Lim, Y. Lu, J. Wang, J. Xu, H. Chen, C. Zhang, M. Hong and X. Liu, *Nature*, 2010, **463**, 1061.
15 T. Wen, W. Luo, Y. Wang, M. Zhang, Y. Guo, J. Yuan, J. Ju, F. Liao and B. Yang, *J. Mater. Chem. C*, 2013, **1**, 1995.
16 W. Luo, Y. Wang, Y. Chen, T. Wen, M. Liu, Y. Wang, F. Liao and J. Lin, *J. Mater. Chem. C*, 2013, **1**, 5711.
17 Q. Dai, M. E. Foley, C. J. Breshike, A. Lita and G. F. Strouse, *J. Am. Chem. Soc.*, 2011, **133**, 15475.
18 J. Wang, F. Wang, C. Wang, Z. Liu and X. Liu, *Angew. Chem. Int. Ed.*, 2011, **50**, 10369.
19 G. S. Yi and G. M. Chow, *J. Mater. Chem.*, 2005, *15*, 4460.
20 G. Chen, H. Qiu, R. Fan, S. Hao, S. Tan, C. Yang and G. Han, *J. Mater. Chem.*, 2012, **22**, 20190.
21 H. Schäfer, P. Ptacek, H. Eickmeier and M. Haase, *Adv. Funct. Mater.*, 2009, **19**, 3091.
22 T. Grzyb and S. Lis, *Inorg. Chem.*, 2011, **50**, 8112.
23 L. Armelao, G. Bottaro, L. Bovo, C. Maccato, M. Pascolini, C. Sada, E. Soini and E. Tondello, *J. Phys. Chem. C*, 2009, **113**, 14429.
24 Y. P. Du, Y. W. Zhang, L. D. Sun and C. H. Yan, *J. Phys. Chem. C*, 2008, **112**, 405.
25 N. Rakov, J. d. A. B. Barbosa, R. B. Guimarães and G. S. Maciel, *J. Alloys Compd.*, 2012, **534**, 32.
26 D. Gao, H. Zheng, X. Zhang, Z. Fu, Z. Zhang, Y. Tian and M. Cui, *Appl. Phys. Lett.*, 2011, **98**, 11907.
27 X. Zhang, D. Gao and L. Li, *J. Appl. Phys.*, 2010, *107*, 123528.
28 M. Shang, G. Li, X. Kang, D. Yang, D. Geng, C. Peng, Z. Cheng, H. Lian and J. Lin, *Dalton Trans.*, 2012, **41**, 5571.
29 Y. P. Du, Y. W. Zhang, Z. G. Yan, L. D. Sun and C. H. Yan, *J. Am. Chem. Soc.*, 2009, **131**, 16364.
30 T. Passuello, F. Piccinelli, M. Pedroni, M. Bettinelli, F. Mangiarini, R. Naccache, F. Vetrone, J. A. Capobianco and A. Speghini, *Opt. Mater.*, 2011, **33**, 643.
31 T. Passuello, F. Piccinelli, M. Pedroni, S. Polizzi, F. Mangiarini, F. Vetrone, M. Bettinelli and A. Speghini, *Opt. Mater.*, 2011, **33**, 1500.
32 T. Grzyb, M. Wedawiak and S. Lis, *J. Alloys Compd.*, 2012, **539**, 82.


Journal of Materials Chemistry C Accepted Manuscript



This journal is © The Royal Society of Chemistry 2015

Please do not adjust margins

33 M. Shang, D. Geng, X. Kang, D. Yang, Y. Zhang and J. Lin, *Inorg. Chem.*, 2012, **51**, 11106.
34 X. Sun, Y. W. Zhang, Y. P. Du, Z. G. Yan, R. Si, L. P. You and C. H. Yan, *Chem. Eur. J.*, 2007, **13**, 2320.
35 G. Yi, Y. Peng and Z. Gao, *Chem. Mater.*, 2011, **23**, 2729.
36 S. Han, R. Deng, X. Xie and X. Liu, *Angew. Chem. Int. Ed.*, 2014, **53**, 11702.
37 L. Tu, X. Liu, F. Wu and H. Zhang, *Chem. Soc. Rev.*, 2015, **44**, 1331.
38 J. Wang, R. Deng, M. A. MacDonald, B. Chen, J. Yuan, F. Wang, D. Chi, T. S. Andy Hor, P. Zhang, G. Liu, Y. Han and X. Liu, *Nat. Mater.*, 2013, **13**, 157.
39 H. Dong, L. D. Sun and C. H. Yan, *Chem. Soc. Rev.*, 2015, **44**, 1608.
40 X. Zhai, S. Liu, Y. Zhang, G. Qin and W. Qin, *J. Mater. Chem. C*, 2014, **2**, 2037.
41 V. Kale, M. Lastusaari, J. Hölsä and T. Soukka, *RSC Adv.*, 2015, **5**, 35858.
42 S. Huang, J. Xu, Z. Zhang, X. Zhang, L. Wang, S. Gai, F. He, N. Niu, M. Zhang and P. Yang, *J. Mater. Chem.*, 2012, **22**, 16136.
43 H. Fu, G. Yang, S. Gai, N. Niu, F. He, J. Xu and P. Yang, *Dalton Trans.*, 2013, **42**, 7863.
44 J. Liu, H. Deng, Z. Huang, Y. Zhang, D. Chen and Y. Shao, *Phys. Chem. Chem. Phys*, 2015, **17**, 15412.
45 G. Chen, T. Y. Ohulchanskyy, R. Kumar, H. Ågren and P. N. Prasad, *ACS Nano*, 2010, **4**, 3163.
46 S. E. Dutton, D. Hirai and R. J. Cava, *Mater. Res. Bull.*, 2012, **47**, 714.
47 Y. Wang, T. Wen, H. Zhang, J. Sun, M. Zhang, Y. Guo, W. Luo, M. Xia, Y. Wang, B. Yang, *J. Phys. Chem. C*, 2014, **118**, 10314.
48 D. J. M. Bevan, J. Mohyla, B. F. Hoskins and R. J. Steen, *Eur. J. Solid State Inorg. Chem.*, 1990, **27**, 451.
49 W. Zheng, P. Huang, D. Tu, E. Ma, H. Zhu and X. Chen, *Chem. Soc. Rev.*, 2015, **44**, 1379.
50 W. B. Pei, B. Chen, L. Wang, J. Wu, X. Teng, R. Lau, L. Huang and W. Huang, *Nanoscale*, 2015, **7**, 4048.


Journal of Materials Chemistry C Accepted Manuscript



Please do not adjust margins

**Table of contents:**

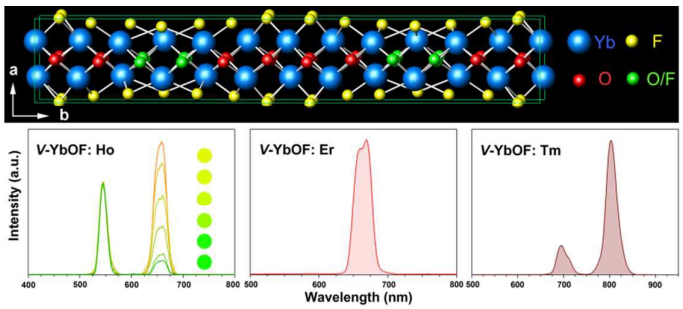


Vernier phase YbOF nanoparticles fabricated via a low temperature fluorination route shows color-tunable and single-band red upconversion luminescences.

Journal of Materials Chemistry C Accepted Manuscript